Do Undiluted Convective Plumes Exist in the Upper Tropical Troposphere?

DAVID M. ROMPS

Department of Earth and Planetary Sciences, Harvard University, Cambridge, Massachusetts

ZHIMING KUANG

Department of Earth and Planetary Sciences, and School of Engineering and Applied Sciences, Harvard University, Cambridge, Massachusetts

ABSTRACT

Using a passive tracer, entrainment is studied in cloud-resolving simulations of deep convection in radiative–convective equilibrium. It is found that the convective flux of undiluted parcels decays with height exponentially, indicating a constant probability per vertical distance of mixing with environmental air. This probability per distance is sufficiently large that undiluted updrafts are negligible above a height of 4–5 km and virtually absent above 10 km. These results are shown to be independent of the horizontal grid size within the range of 3.2 km to 100 m. Plumes that do reach the tropopause are found to be highly diluted.

An equivalent potential temperature is defined that is exactly conserved for all reversible adiabatic transformations, including those with ice. Using this conserved variable, it is shown that the latent heat of fusion (from both freezing and deposition) causes only a small increase in the level of neutral buoyancy near the tropopause. In fact, when taken to sufficiently low pressures, a parcel with an ice phase ends up colder than it would without an ice phase. Nevertheless, the contribution from fusion to a parcel's kinetic energy is quite large.

Using an ensemble of tracers, information is encoded in parcels at the cloud base and decoded where the parcel is observed in the free troposphere. Using this technique, clouds at the tropopause are diagnosed for their cloud-base temperature, specific humidity, and vertical velocity. Using these as the initial values for a Lagrangian parcel model, it is shown that fusion provides the kinetic energy required for diluted parcels to reach the tropopause.

1. Introduction

Despite decades of inquiry, the role of undiluted moist-adiabatic ascent in tropical oceanic deep convection remains a point of debate. Key aspects of the ongoing debate can be captured by four unanswered questions. The first is a simple question of existence: outside of tropical cyclones, do parcels of oceanic boundary layer air convect to the upper troposphere undiluted? The key word here is "undiluted," as in not having entrained environmental air. Since this is a simple question of existence, it might seem easy to prove or refute: simply look and see. However, the evidence to date is ambiguous. The second question is more nuanced: with what distribution of altitudes do undiluted parcels first mix with environmental air? Clearly, this is a more difficult question to answer, but it is one of central importance for the construction of convective parameterizations. Third, what resolution is needed for a cloud-resolving model (CRM) to convincingly demonstrate the existence or nonexistence of undiluted parcels? And, fourth, in the absence of undiluted deep convection, how can we explain the observations of convective plumes at the height of the tropopause?

The notion of undiluted plumes in the upper troposphere owes its origin to the work of Riehl and Malkus (1958). Based on an analysis of moist static energy (MSE) in the upper troposphere, they correctly identified moist deep convection as the source of heat that balances the net cooling from radiation and large-scale ascent. Furthermore, they noted that the MSE of the tropopause was roughly the same as the MSE in the subcloud layer. Since the tropical MSE profile is unimodal in height with a minimum in the middle troposphere, any entrainment of

Corresponding author address: David M. Romps, Harvard University, 416 Geological Museum, 24 Oxford St., Cambridge, MA 02138.
E-mail: davidromps@gmail.com

environmental air into a plume originating from the subcloud layer would lower the plume's MSE below that of the tropopause. Therefore, they argued, the observed convective clouds at the tropopause must be from protected cores of undiluted air rising directly from the subcloud layer. This reasoning, however, is far from iron clad. As noted by Riehl and Malkus, plumes can overshoot their level of neutral buoyancy (LNB), allowing them to reach altitudes with potential temperatures larger than their own. In addition, the latent heat of freezing was not included in their definition of MSE, which can lead to an underestimation of a parcel's final potential temperature (Zipser 2003; Fierro et al. 2009).

In other supporting evidence for the existence of undiluted parcels, Xu and Emanuel (1989) observed that the tropical atmosphere is neutral to undiluted parcels from the top of the subcloud layer. The results of Xu and Emanuel (1989) seem to support a conclusion even stronger than that of Riehl and Malkus (1958): not only do undiluted plumes exist, but they must dominate tropical convection because diluted plumes would not be buoyant. But, it is important to note that the boundary layer is not truly homogenous: air near the surface typically has a higher θ_e than air at the cloud base. Therefore, an observation that the atmosphere is neutral to undiluted ascent from the cloud base also supports the conclusion that the atmosphere is neutral to diluted ascent from closer to the surface. Furthermore, by including the latent heat of fusion in the calculation of convective available potential energy (CAPE), Williams and Renno (1993) found the tropical atmosphere to be quite unstable to undiluted parcels.

The most direct evidence for undiluted ascent would be obtained by measuring the mixing ratio of a conserved tracer in an upper-tropospheric cloud and finding that it is equal to the extremal value typically found only in the subcloud layer. For nonprecipitating convection, two such tracers are total water and liquid-water potential temperature. In fact, many studies have used these two tracers to provide evidence for undiluted cores in midlatitude, midtropospheric, nonprecipitating cumuli (e.g., Heymsfield et al. 1978; Paluch 1979; Jensen et al. 1985). However, these results do not imply the existence of undiluted cores in tropical, upper-tropospheric, precipitating cumuli. To the contrary, Zipser (2003) argues that 35 years worth of observations—including thousands of tropical cumuli observed by aircraft—have not found any conclusive evidence of undiluted ascent in oceanic tropical deep convection outside of tropical cyclones. For example, one hint of undiluted ascent to the upper troposphere comes from measurements of very low ozone mixing ratios at those altitudes, which could be produced by undiluted ascent from the ozone-poor boundary layer

(Kley et al. 1996). But, ozone is not a purely passive tracer: the low values of ozone could be explained by ozone destruction within liquid drops or on the surface of ice particles (Kley et al. 1996) or by destruction of ozone induced by lightning (Wang and Prinn 2000). Despite many efforts, there is still no unambiguous observational evidence of upper-tropospheric, undiluted parcels in unorganized, tropical, oceanic deep convection.

If deep undiluted parcels exist in the real tropics, then they should also show up in faithful cloud-resolving simulations. Fierro et al. (2009) replicated a Tropical Ocean and Global Atmosphere Coupled Ocean–Atmosphere Response Experiment (TOGA COARE) squall line using a cloud-resolving model with a 750-m horizontal resolution and found diluted parcels reaching the tropopause. However, in order to get a faithful representation of the squall line, they had to cool the free troposphere well below the observed temperatures. This raises the possibility that 750 m is too coarse to resolve undiluted parcels, so a cooler troposphere was needed to get the diluted parcels to the height of the observed clouds. Indeed, when studying a squall line in a CRM over a range of grid spacings, Bryan et al. (2003) found that a resolution of at least 100 m is required to resolve the low-wavenumber end of the inertial subrange. Even at 100 m, they found that many aspects of the simulation had still not converged. Kuang and Bretherton (2006) studied deep convection in a cloud-resolving model at a 100-m resolution and found no significant flux of undiluted air in the upper troposphere. However, for unorganized tropical convection, where the integral scale may be smaller than for a squall line, smaller grid spacings may be required to achieve convergence. During flights through cumulus clouds, MacPherson and Isaac (1977) found that the $-\frac{5}{3}$ law for the inertial subrange was satisfied for wavelengths less than 70 m. For a model to resolve eddies on that scale, a grid spacing somewhat smaller than this may be needed.

The question of where an undiluted parcel first entrains environmental air is of central importance to convective parameterizations. In the model by Kain and Fritsch (1990), mixtures of plume and environment are immediately and homogeneously mixed into the plume itself, guaranteeing that there is never any undiluted mass flux above the cloud base. In other words,

$$U(p) = 0, \quad \forall \quad p < p_b, \tag{1}$$

where $U(p)$ is the undiluted cloud flux at pressures less than the cloud base pressure p_b. In stark contrast, Raymond and Blyth (1986) assume in their model that cloud-base air rises undiluted with an equal probability density to any pressure level between the cloud base and the level of neutral buoyancy for an undiluted parcel. In

the case of deep convection, this would imply that the flux of undiluted cloud decreases linearly in pressure all the way to the vicinity of the tropopause,

$$U(p) = U(p_b)\left(1 - \frac{p_b - p}{p_b - p_t}\right), \qquad (2)$$

where p_t is the pressure of the undiluted level of neutral buoyancy. Motivated by the finding that stratification affects entrainment rates (Bretherton and Smolarkiewicz 1989), Emanuel and Živković-Rothman (1999) assume in their model that the flux of undiluted air is modified by its buoyancy as follows:

$$U(p) = U(p_b)\left(1 - \frac{p_b - p + \Lambda^{-1}\int_p^{p_b} dp'|dB/dp'|}{p_b - p_t + \Lambda^{-1}\int_{p_t}^{p_b} dp'|dB/dp'|}\right). \qquad (3)$$

Here $B(p')$ is the buoyancy of an undiluted parcel lifted to pressure level p', and Λ is a constant that must be tuned. Applied to the same atmospheric sounding, these three models would produce very different undiluted fluxes, reflecting the large uncertainty as to where these clouds first entrain environmental air.

The approach of this paper is to study undiluted clouds in a CRM at various horizontal resolutions. Section 2 presents a technique using passive tracers that allows us to diagnose a parcel's net entrainment, to detect undiluted parcels, and to read off the original cloud-base properties of any convecting parcel in the free troposphere. Section 3 describes the model and the setup of the simulations. The results of these runs, and their dependence on resolution, are discussed in section 4. Section 5 presents two pieces of evidence that undercut the standard argument in favor of the existence of undiluted plumes. First, deep convection does reach the tropopause in the CRM, but it is highly diluted. Second, even the level of neutral buoyancy for a theoretical undiluted plume falls well short of the tropopause. Section 6 employs an entraining parcel model to explain how a diluted plume can reach the tropopause, and evidence is given that fusion plays a key role in making this possible. Finally, section 7 summarizes the conclusions.

2. Purity tracer

The use of conserved scalars as a way to diagnose convective mixing is not new. In simulations of nonprecipitating convection, changes in the conserved variables of total water and liquid-water potential temperature can be used to diagnose effective entrainment

and detrainment rates (e.g., Siebesma and Holtslag 1996). In the case of deep convection, the fallout of precipitation causes neither total water nor liquid-water potential temperature to be conserved. As an alternative, Kuang and Bretherton (2006) diagnose entrainment rates in deep convection using moist static energy (MSE), which is approximately conserved even in the presence of precipitation. One drawback of this technique is that the purity of a parcel—the ratio of original cloud-base air to the total air in the parcel—cannot be estimated without other assumptions. Because the environmental MSE profile decreases with height in the lower half of the troposphere, a parcel observed in the middle troposphere with an MSE less than the cloud-base value may have entrained a lot of air near the cloud base or relatively little farther up. Another difficulty is caused by the fact that the environmental MSE profile is close to the undiluted parcel's MSE near the bottom and top of the troposphere. This makes it impossible to differentiate between a nearly undiluted parcel and a parcel that is heavily diluted with air from those two places.

An alternative technique is to introduce artificial passive tracers, whose sources and sinks can be carefully controlled. Bretherton and Smolarkiewicz (1989) use tracers to measure entrainment and detrainment for an individual convective event. In that study, the tracers are initialized once and then their distribution at a later time is used to diagnose the total entrainment and detrainment in the intervening period of convection. In another approach, Cohen (2000) and Yasunaga et al. (2004) inject tracers throughout the troposphere at regular intervals, allowing them to diagnose entrainment and detrainment rates for entire ensembles of clouds.

In this study, we are less interested in entrainment and detrainment per se than we are in the dilution of the subcloud-layer air. Consequently, we need a tracer that can track a parcel's purity, that is, the fraction of the parcel that recently originated in the subcloud layer. For a simulation of a single cloud, the way to proceed is fairly straightforward. Before the cloud develops at the cloud base, initialize the passive tracer to a constant value of one kilogram of tracer per kilogram of dry air below the cloud base and zero kilograms of tracer per kilogram of dry air above the cloud base. At later times, the value of the tracer in a cloudy grid cell records the fraction of dry air that originated in the subcloud layer. It is natural to call this tracer the "purity tracer" or, simply, "purity."

In the case of radiative–convective equilibrium (RCE), as opposed to a single cloud, it is necessary to introduce sources and sinks of purity. To guarantee that any parcel passing up through the cloud base carries a purity value of one, the purity is set to one everywhere below the cloud base at every time step. Above the cloud base, it is

necessary to delete purity in a way that guarantees two desirable properties: that the purity tracer records the fraction of air *recently* transported from below the cloud base and that the purity tracer is *passively* transported within all active convection.

To this end, each grid cell above the cloud base is equipped with a clock that is incremented at every time step. Every time the clock in that grid cell reaches a time τ, the purity and the clock are both reset to zero. So long as τ is smaller than the time it takes convection to return to those grid cells, each convecting cloud will entrain environmental air with zero purity. This guarantees that the purity tracer will faithfully reflect the presence of *recent* subcloud-layer air.

To avoid zeroing the purity within an actively convecting cloud, the clock is also reset to zero every time the grid cell hosts cloudy updrafts. Here, cloudy updrafts are defined as the presence of condensed water at a mass fraction greater than 10^{-5} kg kg^{-1} and a vertical velocity greater than 1 m s^{-1}. According to this definition, eddies within a cloud can cause parcels to switch back and forth between the classifications of cloudy updraft and environmental air. But, so long as τ is greater than the time scale of eddies, the purity will not be reset in an active cloud. This guarantees that purity is *passively* transported by convection.

The key, therefore, is to choose a value for τ that is smaller than the local recurrence time for convection and greater than the eddy turnover time. For this purpose, we use a value of one hour. Watching animations of the purity tracer in a cloud-resolving model has confirmed the appropriateness of this choice. In simulations of RCE, the troposphere is kept clear of vestigial purity, but the purity tracer does not zero out until after the local convective event has finished.

The utility of the purity tracer is twofold. First, it can give us a very clear picture of where in the free troposphere undiluted parcels first mix with environmental air. This is accomplished by recording the flux at each height of undiluted cloudy updrafts, which are defined as having a sufficiently high purity to qualify as undiluted. Throughout this study, we use a threshold of 80%. This threshold is chosen to be relatively low so as to give parcels ample opportunity to qualify as undiluted; even with this lax definition, we will find that undiluted parcels are rare. Higher thresholds reduce the number of undiluted parcels but do not otherwise affect the results in any significant way.

The second use for the purity tracer is as a decoder for information stored in additional tracers. This is best illustrated by an example. Let us add a second tracer that is treated in the same way as the purity tracer except for one difference: instead of being set to one in the subcloud

layer, it is set to equal to the local equivalent potential temperature, θ_e. If a parcel remains undiluted as it travels through the troposphere, then its cloud-base θ_e can be read off from the mixing ratio of this second tracer. For a diluted parcel, we can take advantage of the fact that both tracers get diluted by the same fraction since the parcel entrains environmental air with zero values of both tracers. This means that the value the second tracer had at the cloud base z_b can be decoded by dividing by the purity:

$$r_{\theta_e}(z_b) = \frac{r_{\theta_e}(z)}{r_{\mathrm{purity}}(z)}.$$

This is useful for diagnosing the cloud-base θ_e of parcels that reach the tropopause or, for that matter, any height in the troposphere.

3. Model and setup

For the cloud-resolving simulations, we use Das Atmosphärische Modell (DAM) (Romps 2008). This is a three-dimensional, fully compressible, finite-volume, cloud-resolving model. Integration uses a split-time scheme whereby a large time step is advanced using third-order Runge–Kutta, and each Runge–Kutta step is subdivided into smaller steps for the integration of fast acoustic and gravity modes (Klemp et al. 2007). Microphysics is treated using the Lin–Lord–Krueger six-class microphysics scheme (Lin et al. 1983; Lord et al. 1984; Krueger et al. 1995). Both shortwave radiation and longwave radiation are modeled using the Rapid Radiative Transfer Model (RRTM) (Clough et al. 2005; Iacono et al. 2008). The conservative flux advection is performed on the Arakawa-C grid using a third-order stencil and a flux limiter to maintain positive definite scalars. We do not supplement numerical diffusion of scalars with any other model of subgrid diffusion. This choice was made to increase the odds of producing undiluted parcels and because previous simulations showed a more realistic distribution of lower-tropospheric cloud in the absence of such a model.

The simulations are run in a 25.6-km-wide cubical domain and periodic lateral boundary conditions. One simulation was also run on a larger horizontal domain to confirm that the results are independent of domain size. In all simulations, the lower boundary is set to an ocean with a temperature of 300 K. The shortwave radiation flux and zenith angle are specified to give the average daily normal flux at the equinoctial equator using an incidence angle whose cosine is equal to the daily normal-flux-weighted average. Using an isotropic 200-m grid, the atmosphere is run to a steady state over several weeks of model time. Over two more weeks, the simulation is run with tracers to gather statistics on the steady-state
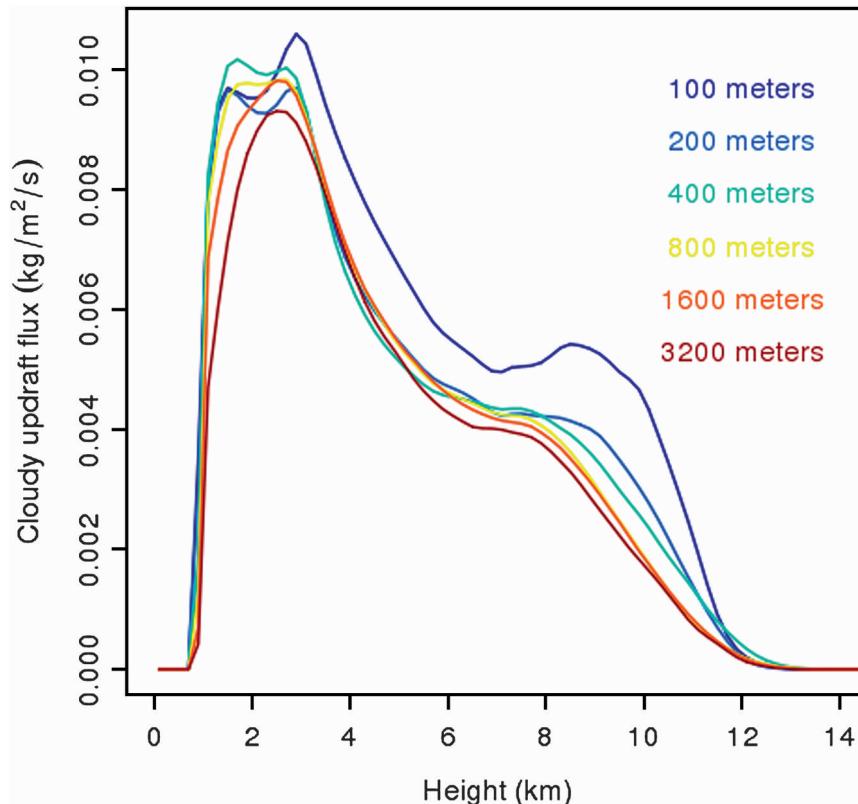
FIG. 1. Cloudy updraft flux at different horizontal resolutions.

convection. To study the effect of resolution on these statistics, the same 25.6-km-cubed domain is restarted from the 200-m simulation using different horizontal resolutions. Using the same 200-m vertical resolution throughout, simulations are run with tracers for two weeks at horizontal resolutions of 200, 400, 800, 1600, and 3200 m. Results shown in the next section for these resolutions are averaged over the two-week periods. In addition, a simulation with a 100-m horizontal resolution and the same 200-m vertical spacing and 25.6-km-cubed domain is run for three days. Although the data from this run is of lower quality due its shorter three-day averaging, it is included in many of the figures because of its relevance to the question of resolution dependence.

4. Results

After running the simulations as described, the first order of business is to check that all six of the simulations are deeply convecting. Figure 1 shows the vertical profiles of the cloudy updraft flux in all six runs. It is clear that all of the runs contain deep convection. Furthermore, the six simulations exhibit very similar profiles of cloudy updrafts. This is as expected since the convection in all six runs must balance similar profiles of

radiative cooling. Figure 2 shows the temperature profile and dewpoint (the two solid lines) for the simulation with a 200-m horizontal resolution. The low mixing ratio of water vapor in the lower stratosphere is a numerical artifact of the nonmonotonic advection scheme acting on steep gradients over the course of several weeks. The dashed line gives the moist adiabatic lapse rate with fusion; this yields a convective available potential energy (CAPE) of 1300 J kg^{-1}, in the middle of the ranges observed by Williams and Renno (1993). Since no mean wind has been prescribed, there is a relatively large temperature difference between the sea surface and the surface air temperature. This relatively cool surface air temperature, which also causes a somewhat higher moist lapse rate, gives a melting line at 3.3 km. These effects, plus the absence of large-scale ascent, put the tropopause at about 13.8 km. Although the temperature is cooler and the melting line and tropopause lower than is typically found over the warm pool, any qualitative results on mixing in convective plumes or on the relationship between convection and the tropopause should be largely independent of these details.

To enable a study of undiluted cloudy updrafts, we have binned the cloudy updraft mass flux according to height and purity. At every time step, the vertical mass
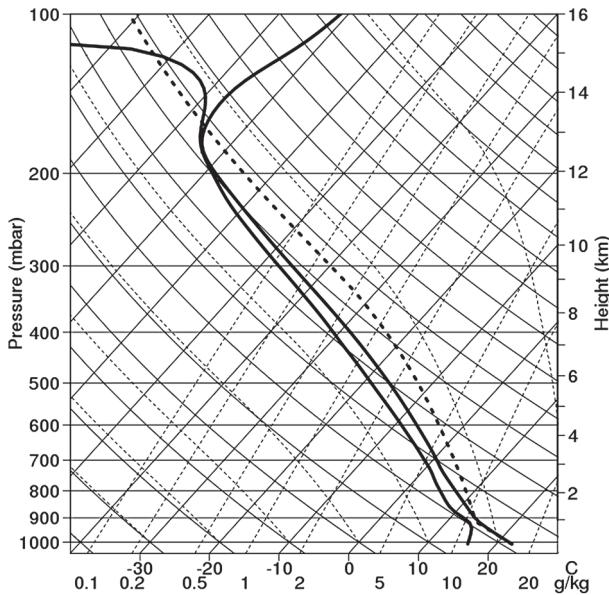
FIG. 2. Environmental profile of the 200-m simulation: given by the thick solid line to the right in this skew T–log$p$ diagram. The thick solid line to the left is the dewpoint temperature using ice saturation below 0°C. The thick dashed line denotes a moist adiabat beginning at the surface with average temperature and water vapor.

transport in every cloudy-updraft grid cell is added to a matrix element corresponding to that grid cell's height and purity. The resulting matrix, divided by the integration time, is shown in Fig. 3 for the 200-m resolution run. The dominant feature of this plot is the decreasing purity of updrafts with height. In the upper left corner of the figure, there is a thin, short band of flux at a purity of one that is an artifact of the advection scheme being positive definite, but not total variation diminishing. Near the cloud base, where purity values are high, some values of purity exceed one by small amounts, and those values have been lumped into the bin for unit purity.

With this purity-binned flux data, it is a simple matter to calculate the flux-weighted average purity of the cloudy updrafts. The mean purity values are shown in Fig. 4 at every height for all six simulations. It is particularly striking in this figure just how small the ratios are throughout most of the troposphere. Everywhere above three kilometers, cloudy updrafts are comprised mostly of air entrained from above the cloud base.

One trend, apparent in Fig. 4, is that the purity of cloudy updrafts throughout most of the troposphere *decreases* with increasing resolution. Although we are not currently in a position to ascertain why, two possible explanations seem likely. One is that the increased Reynolds number with higher resolution allows for more efficient turbulent entrainment of environmental air into cloudy updrafts. Another plausible explanation would be that the finer horizontal resolution allows for

skinnier updrafts for which the perturbation pressure field is less able to counteract the buoyancy force. This would allow these narrow parcels to convert buoyancy into vertical velocity more efficiently, allowing relatively diluted parcels to qualify as cloudy updrafts.

While interesting, the average purity of cloudy updrafts does not tell us much about the undiluted updrafts. Here, we define a parcel—or grid point—as undiluted when its purity tracer is greater than 80%. Figure 5 shows the fraction of cloudy updraft flux that is undiluted in each of the six simulations. This graph is remarkable for the near-total absence of undiluted updrafts in the middle to upper troposphere: the fraction of cloudy updrafts that are undiluted is less than 1% above about 4–5 km in all runs. Furthermore, there is no systematic trend in the undiluted fluxes with increasing resolution, suggesting that these results may be safely extrapolated to a higher resolution.

We are also in a position to compare the results of the cloud-resolving simulation to Eqs. (1)–(3). The solid line in Fig. 6 plots the flux of undiluted cloudy updrafts for the run with the 200-m horizontal resolution. This curve is remarkable for its nearly perfect exponential decay with respect to height. This suggests a stochastic process whereby an undiluted parcel has a constant probability per height of becoming diluted with environmental air. For the 200-m run, the slope of the natural logarithm of the undiluted flux (>80% pure) is 1.85 km^{-1}. The values for the other runs fall within the range of 1.85 ± 0.25 km^{-1} with no systematic trend with increasing resolution. Note that the central value of 1.85 km^{-1} corresponds to a characteristic mixing distance of 540 m. To test the possibility that the small domain size is having some effect on these results, we ran the 400-m resolution run for an additional three days on a 102.4-km-wide square domain and obtained an exponential decay of 1.90 km^{-1}.

Models of convection that employ a single entraining plume, such as that of Kain and Fritsch (1990), predict that there are no strictly undiluted updrafts above the cloud base. Recall, however, that we are using a rather generous definition of "undiluted": no more than 20% environmental air. Under this definition, the profile of undiluted mass flux in the Kain–Fritsch model would drop discontinuously to zero at the height at which the plume fails to satisfy this definition of undiluted. Needless to say, the solid line in Fig. 6 has no such discontinuity.

The dashed line in Fig. 6 corresponds to Eq. (2)—or, equivalently, Eq. (3) with Λ taken to infinity—with the value of $U(p_b)$ taken from the cloud-resolving simulation. At the other extreme is Eq. (3) with Λ set to zero, as depicted by the dotted line. Both of these equations overestimate the undiluted flux by orders of magnitude. Fortunately, the invariance of the exponential decay with increasing resolution suggests that the relation
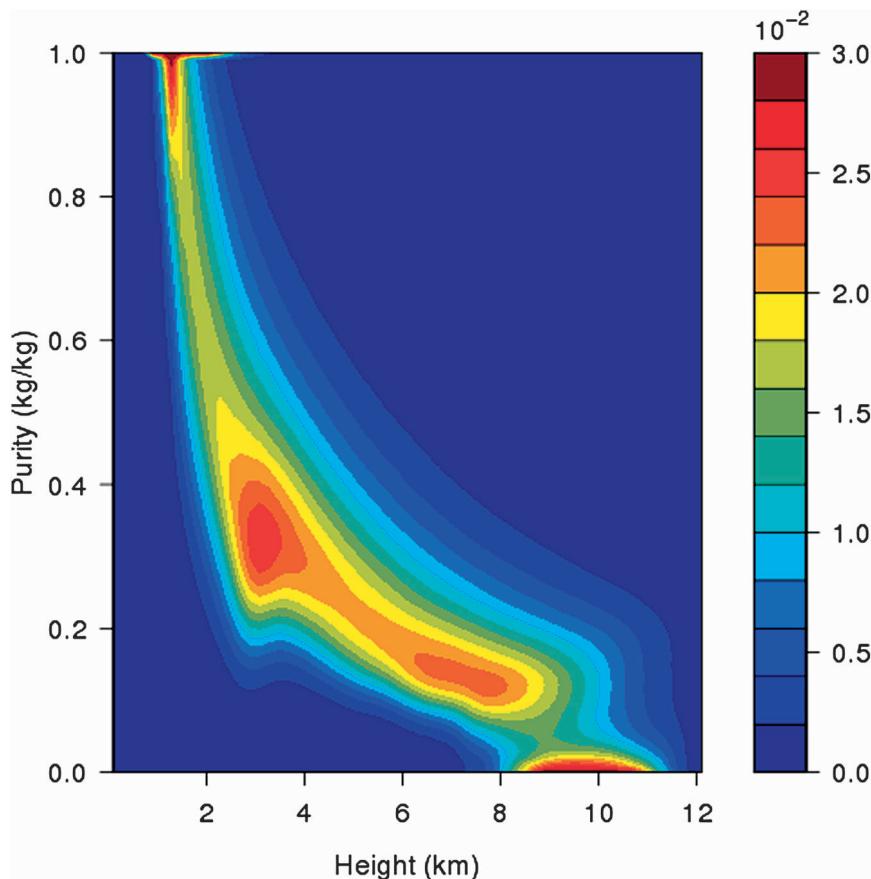
FIG. 3. Cloudy updraft mass-flux density (kg m^{-2} s^{-1} per kg kg^{-1} of purity interval) for the 200-m run binned according to height and purity.

$$U(z) = U(z_b)e^{-\lambda z}, \quad \lambda = 1.85 \, \text{km}^{-1},$$

may be applicable to real tropical RCE and so may be used in the parameterizations of Raymond and Blyth (1986) and Emanuel and Živković-Rothman (1999) in place of Eqs. (2) and (3).

How faithful, then, are these RCE simulations to the behavior of deep convection in the tropics? For example, the simulations presented here cannot simulate mesoscale organization or other large-scale influences. Fortunately, the process of interest here—mixing between the cloud and its environment—should depend on the large-scale environment mainly through the environment's effect on cloud size. The larger the cloud, the lower the probability is that a cloudy parcel will mix with environmental air. Quantitatively, the mixing rate λ should scale as $1/D$, where D is the diameter or width of the cloud.

From measurements gathered during the Global Atmospheric Research Program's Atlantic Tropical Experiment (GATE), LeMone and Zipser (1980) studied "cores" defined as contiguous flight-path observations

of vertical velocities greater than 1 m s^{-1} for more than 500 m. Collecting these statistics in the altitude range from 4.3 to 8.1 km, they found a cumulative distribution that has been roughly replicated by the dashed line in Fig. 7. LeMone and Zipser found that 0.1% of the cores during GATE at these heights had a width greater than or equal to about 5.4 km. In the 200-m simulation, 0.1% of the cores in this height range had a width greater than or equal to 3.3 km; the full distribution is given by the solid line in Fig. 7. Overall, the largest cores observed during GATE were about twice as wide as the largest cores observed in the 200-m simulation. Therefore, the best guess of the mixing rate for the deep convective clouds in GATE would be $\lambda = 1.85/2 = 0.93$ km^{-1}. This corresponds to a reduction in the undiluted flux by a factor of 0.4 once every kilometer, which is still a sufficiently fast extinction rate to make undiluted parcels irrelevant to deep convection in the upper troposphere.

Finally, it is important to emphasize that the decay rate of undiluted flux, λ, is not the same entity as the entrainment rate diagnosed in many other studies (e.g., Siebesma and Cuijpers 1995). The decay rate of undiluted
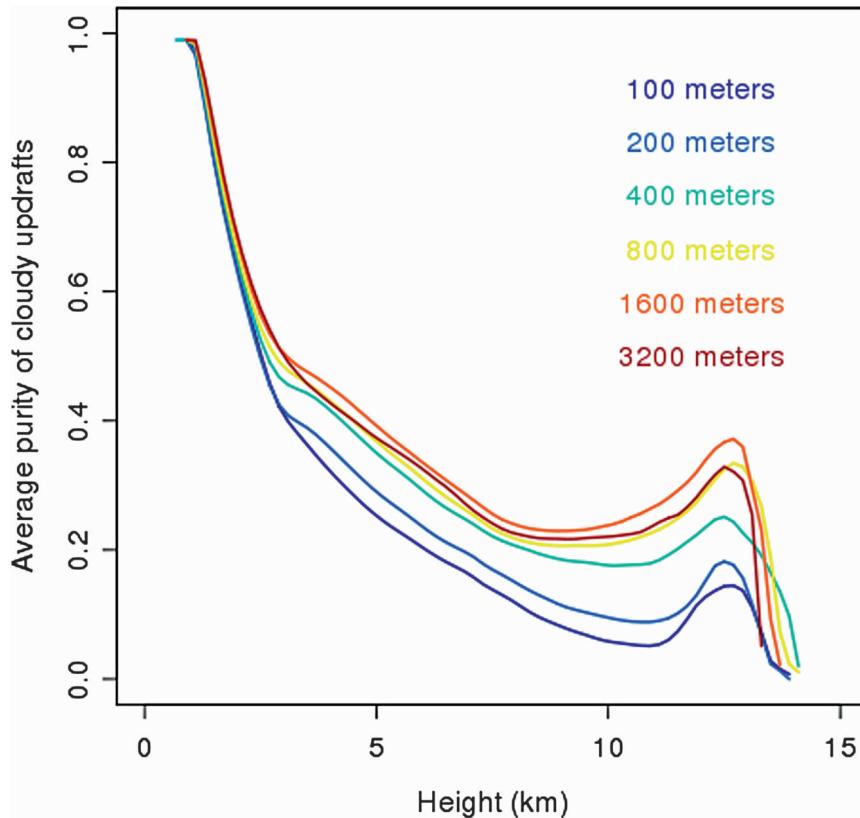
FIG. 4. The average purity of the cloudy updraft flux.

flux is a measure of the probability of a mixing event: for a sufficiently stringent definition of "undiluted" any positive amount of entrained air will cause a dilution. In contrast, entrainment is a function of the probability of a mixing event and the amount of environmental air involved in that mixing event.

5. Maximum level of neutral buoyancy

Another important result from the simulations is the observation that cloudy updrafts reach the tropopause even though they are highly diluted. For example, in the simulation using a 200-m horizontal resolution, a cloudy updraft penetrated the tropopause sometime between 48 and 54 h into the run. When it reached the tropopause, this cloud had a purity of only 50%. How is it possible that such a diluted cloud made it to the tropopause? One possibility is that the level of neutral buoyancy (LNB) for an undiluted parcel is actually higher than the tropopause; if this were the case, a parcel could entrain some low-θ_e midtropospheric air and still have

a LNB at the tropopause. This section is devoted to testing this hypothesis.

First, however, we must define what we mean by "a parcel's level of neutral buoyancy." For a moist parcel, the LNB is dependent on the details of condensate fallout. To avoid shortchanging our parcels, we will calculate the maximum level of neutral buoyancy LNB_{max}, which we define as the maximum LNB a parcel can attain through an ascending trajectory and any sequence of condensate fallout. This maximum LNB is approximately achieved by the retention of condensates (so as to benefit from their heat capacity) followed by the fallout of condensates near the end of its trajectory (so as to lighten the load and rise a bit farther). The restriction that the parcel follow a strictly ascending trajectory excludes the possibility that the parcel could overshoot its final LNB and, in so doing, entrain warmer overlying air or extract further internal energy from the condensates before they fall out. We calculate LNB_{max} as the height at which the density of a parcel times one minus its mass fraction of condensates equals the density of the environment:

$$LNB_{max} = z \quad \text{s.t.} \quad \left\{ (1 - q_l - q_s)\rho \big|_{\text{ascent of parcel to } z \text{ with no fallout}} = \rho \big|_{\text{environment at } z} \right\}.$$
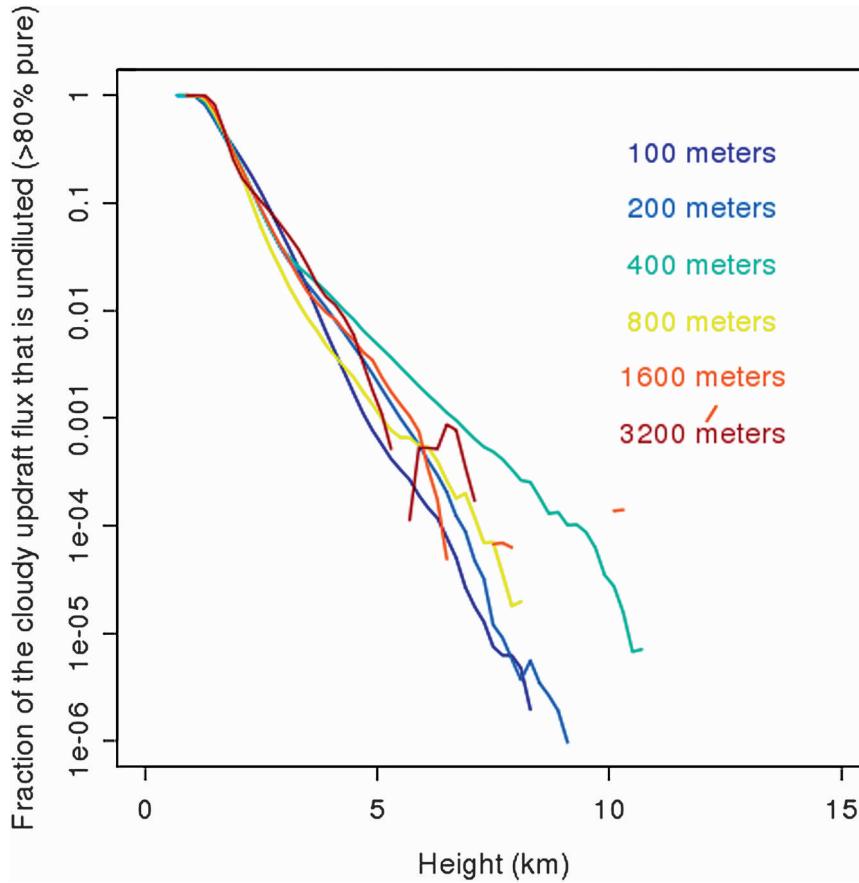
FIG. 5. Ratio of the undiluted cloudy updraft flux to the total cloudy updraft flux.

The calculation of $\text{LNB}_{\max}$ requires that we have a way to calculate the state of a parcel (in particular, q_l, q_s, and ρ) at various different pressures (i.e., heights in the atmosphere). For this purpose, it is useful to have an equivalent potential temperature θ_e that is strictly conserved for all adiabatic and reversible transformations, including those that involve freezing and deposition. To derive θ_e, we begin with the specific entropies of dry air, water vapor, liquid water, and solid water, denoted by subscripts a, v, l, and s, respectively:

$$s_a = c_{pa} \log\left(\frac{T}{T_{\text{trip}}}\right) - R_a \log\left(\frac{p_a}{p_{\text{trip}}}\right);$$

$$s_v = c_{pv} \log\left(\frac{T}{T_{\text{trip}}}\right) - R_v \log\left(\frac{p_v}{p_{\text{trip}}}\right) + s_{0v};$$

$$s_l = c_{vl} \log\left(\frac{T}{T_{\text{trip}}}\right);$$

$$s_s = c_{vs} \log\left(\frac{T}{T_{\text{trip}}}\right) - s_{0s}.$$

Here c_v and c_p are the heat capacities at constant volume and pressure, p_{trip} and T_{trip} are the pressure and temperature of the triple point, p_a and p_v are the partial pressures of dry air and vapor, and s_{0v} and s_{0s} are the specific entropies of vapor and solid at the triple point.[1] Using r to denote mixing ratios, the entropy per dry-air mass,

$$s_a + r_v s_v + r_l s_l + r_s s_s = (c_{pa} + r_v c_{pv} + r_l c_{vl} + r_s c_{vs})$$
$$\times \log\left(\frac{T}{T_{\text{trip}}}\right) - R_a \log\left(\frac{p_a}{p_{\text{trip}}}\right)$$
$$- r_v R_v \log\left(\frac{p_v}{p_{\text{trip}}}\right) + r_v s_{0v} - r_s s_{0s},$$

is invariant under adiabatic and reversible transformations. Dividing by c_{pa}, exponentiating, and multiplying

---

[1] Das Atmosphärische Modell uses the values $c_{va} = 719$, $c_{vv} = 1418$, $c_{vl} = 4216$, $c_{vs} = 2106$, $R_a = 287.04$, $R_v = 461.4$, $p_{\text{trip}} = 611.65$, $T_{\text{trip}} = 273.16$, $E_{0v} = 2.374 \times 10^6$, $E_{0s} = 3.337 \times 10^5$, $s_{0v} = E_{0v}/T_{\text{trip}} + R_v$, and $s_{0s} = E_{0s}/T_{\text{trip}}$, all in mks units.
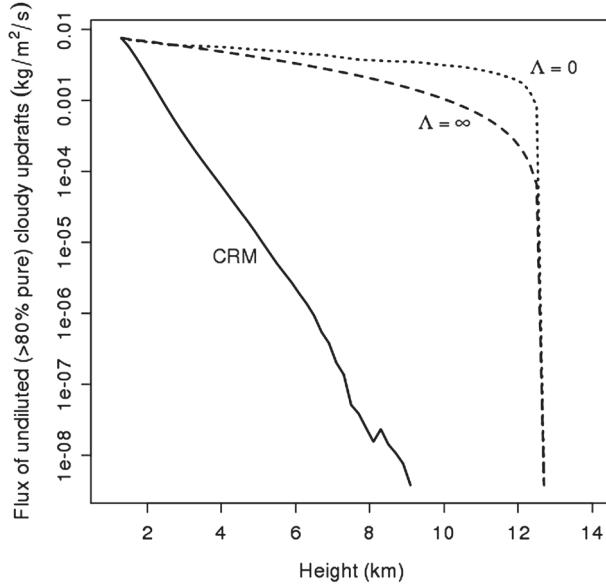
FIG. 6. Flux of undiluted (>80% pure) cloudy updrafts in the CRM with 200-m resolution, the model of Raymond and Blyth (1986) ($\Lambda = \infty$), and the model of Emanuel and Živković-Rothman (1999) with $\Lambda = 0$.

by $T_{\text{trip}}(p_0/p_{\text{trip}})^{R_a/c_{pa}}$ produces another invariant that we define as θ_e:

$$\theta_e \equiv T \left(\frac{p_0}{p_a}\right)^{R_a/c_{pa}} \left(\frac{T}{T_{\text{trip}}}\right)^{(r_v c_{pv} + r_l c_{vl} + r_s c_{vs})/c_{pa}} \left(\frac{p_{\text{trip}}}{p_v}\right)^{r_v R_v/c_{pa}}$$

$$\times \exp\left[\frac{(r_v s_{0v} - r_s s_{0s})}{c_{pa}}\right]. \tag{4}$$

Note that this reduces to the potential temperature for dry air in the absence of water. It is straightforward to check that the invariant θ'_e used by Hauf and Höller (1987) is related to this θ_e by

$$\theta'_e = (T_{\text{trip}}^{r_t c_{vl}/c_{pa}} \theta_e)^{c_{pa}/(c_{pa}+r_l c_{vl})},$$

where $r_t = r_v + r_l + r_s$ is the total mixing ratio of water. The definition used by Emanuel (1994) is the same as the one used by Hauf and Höller (1987), but with no accounting for the solid phase; that is, $c_{vs} \to c_{vl}$ and $s_{0s} \to 0$.

Given the definitions of θ_e and the saturation vapor pressures,[2] a root solver can be used to calculate the properties of a parcel that has been transformed adiabatically and reversibly to any pressure. As the parcel is

---

[2] The saturation vapor pressures over liquid and solid water are, respectively, $p_v^{*,l} = p_{\text{trip}}(T/T_{\text{trip}})^{(c_{pv}-c_{vl})/R_v} \exp\{[(E_{0v}-(c_{vv}-c_{vl})T_{\text{trip}})/R_v][(1/T_{\text{trip}})-(1/T)]\}$; $p_v^{*,s} = p_{\text{trip}}(T/T_{\text{trip}})^{(c_{pv}-c_{vs})/R_v} \exp\{[(E_{0v}+E_{0s}-(c_{vv}-c_{vs})T_{\text{trip}})/R_v][(1/T_{\text{trip}})-(1/T)]\}$.
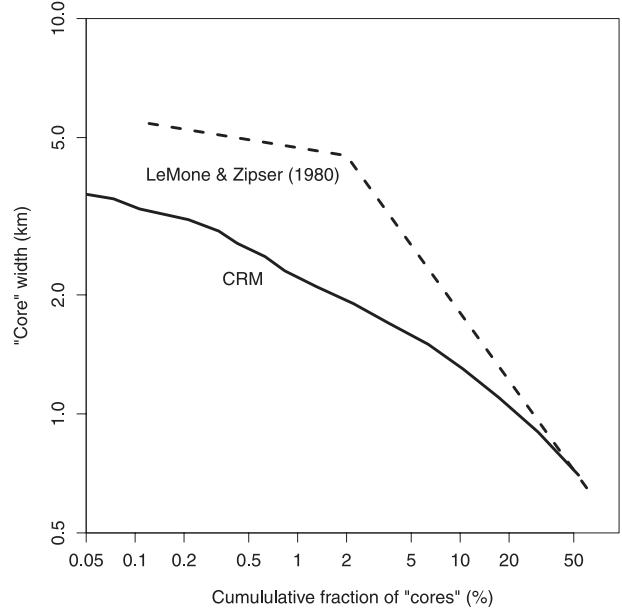

FIG. 7. Cumulative distributions of the "core" widths (defined as the length of contiguous $w > 1$ m s^{-1} greater than 500 m in length along a horizontal line) as reported for GATE by LeMone and Zipser (1980) (dashed) and for the CRM (solid).

expanded reversibly to lower pressures, it goes through four stages: subsaturation, saturation with respect to liquid, the isothermal triple point with all three phases present, and then saturation with respect to solid water. In the first, second, and fourth stages, the root solver is used to find the temperature of the parcel. In the third stage, for which the temperature is known to be 273.16 K, the root solver is used to find the partitioning of condensates into liquid and solid. Once the root solver has been used in this way, we can calculate the density of the parcel and, given an environmental profile, its LNB$_{\text{max}}$.

We have proceeded with this calculation using the mean profiles from the 200-m simulation and initializing the parcel with the mean temperature and saturation water vapor at the cloud base. To test the effects of fusion, we have repeated the calculation for an adiabatic parcel without fusion. In the following, we will refer repeatedly to parcels "with fusion" and "without fusion." Parcels with fusion are those for which a solid phase of water is allowed and c_{vs} and s_{0s} take their standard values. Parcels without fusion can be thought of as having no solid phase of water or, equivalently, a solid phase that is indistinguishable from the liquid phase, which is accomplished by setting $c_{vs} = c_{vl}$ and $s_{0s} = 0$. We have also repeated both of these calculations (fusion and no fusion) using an entrainment rate that yields the 50% diluted parcel observed in the 200-m simulation: $-\log(50\%)/(14\,000 - 1000) = 5.33 \times 10^{-5}$ m^{-1}. For simplicity, we use the approximation that θ_e mixes linearly.
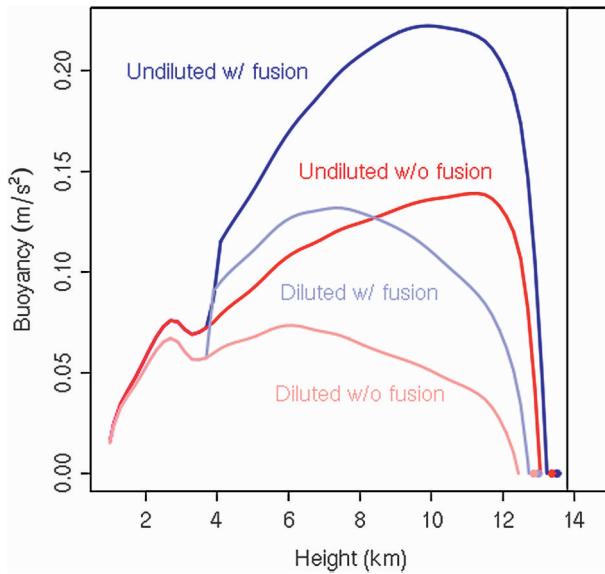
FIG. 8. Buoyancy of a parcel with θ_e equal to the average θ_e^* at the cloud base rising either undiluted (primary colors) or diluted with $\epsilon = 5.33 \times 10^{-5}$ m^{-1} (pastel colors) and either with fusion (bluish) or without (reddish). The colored circles indicate the locations of the respective LNB$_{max}$.

The results from all four of these calculations (fusion and no fusion; undiluted and diluted) are illustrated in Fig. 8. The curves with primary colors (red and blue) are the undiluted trajectories and the curves with pastel colors (pink and light blue) are the entraining trajectories. The bluish curves (blue and light blue) are with fusion and the reddish curves (red and pink) are without. The colored circles indicate the LNB$_{max}$ for each of the parcels and the thin vertical line denotes the height of the tropopause. The maximum levels of neutral buoyancy for all of the parcels—including even the undiluted parcel with fusion—lie below the tropopause. This disproves the hypothesis that diluted parcels reach the tropopause because the LNB$_{max}$ for the undiluted parcel is well above the tropopause—to the contrary, it is below.

It is very interesting to note that the effect of entraining at a rate of 5.33×10^{-5} m^{-1}—producing a one-to-one mixture of cloud-base and environmental air—is to reduce the LNB$_{max}$ by only 500 m. Even more surprising is the fact that the effect of fusion is to raise the LNB$_{max}$ for the undiluted parcel by only 140 m. Therefore, if fusion is to play a role in getting parcels to the tropopause, it will not be through an increase in the level of neutral buoyancy.

There are two reasons why fusion has such a small effect on the LNB$_{max}$. The first is due to the high static stability of the environment in the vicinity of the tropopause. When 0.01 kg kg^{-1} of solid water is generated by a parcel, the consequent release of the latent heat of fusion generates a roughly 3-K increase in the parcel

temperature. Near the tropopause, where the lapse rate is zero, this raises the level of neutral buoyancy by only 300 m.

The second reason has to do with the difference in heat capacity between liquid and solid water. Ice has only half the heat capacity of liquid water: 2106 J kg^{-1} compared to 4216 J kg^{-1}. As an ice cloud expands and cools, the ice releases less sensible heat than the liquid water would have. Put another way, ice has a smaller "thermal inertia" than liquid water. To quantify this effect, consider a parcel with constant gas constant R and heat capacity c_p that transforms from p_1, T_1 to p_2, T_2. If the transformation were adiabatic, then these pressure and temperatures would be related by the invariance of the potential temperature. On the other hand, if heat were added between these two states, then the appropriate relation becomes

$$T_2 = T_1 \left(\frac{p_2}{p_1} \right)^{R/c_p} \exp \left(\int_1^2 \frac{dQ}{c_p T} \right).$$

To compare parcels with and without fusion, we will use p_f and T_f to denote the effective pressure and temperature at which the latent heat of fusion is added to an expanding parcel. The temperature difference between a parcel with and without fusion at a pressure p smaller than p_f may be approximated as

$$\Delta T \simeq q_t T \left[\frac{L_m(T_f)}{c_{pa} T_f} - \frac{R_a(c_{vl} - c_{vs})}{c_{pa}^2} \log \left(\frac{p_f}{p} \right) \right].$$

For pressures not much lower than p_f, the release of latent heat dominates, causing the parcel to be warmer than it would otherwise be. But, for a sufficiently small pressure, the temperature difference actually crosses zero and goes negative.

Using the equivalent potential temperature in Eq. (4), we can calculate the effect that fusion has on a parcel's temperature. We begin with a parcel at 1000 mb and 80% relative humidity and then adiabatically and reversibly lower its pressure. Using the conservation equation $\theta_e = $ const, we can solve for the temperature of the parcel at each pressure. We perform this calculation twice: once for a parcel with fusion and once for a parcel without fusion; that is, $s_{0s} = 0$ and $c_{vs} = c_{vl}$. The differences in parcel temperatures (fusion minus no fusion) are shown in Fig. 9 for initial parcel temperatures between 280 and 310 K. As expected, the temperature deviations decrease toward zero in the upper troposphere. For example, a parcel beginning at 1 bar with a temperature of 300 K and a relative humidity of 80% has its temperature boosted by fusion
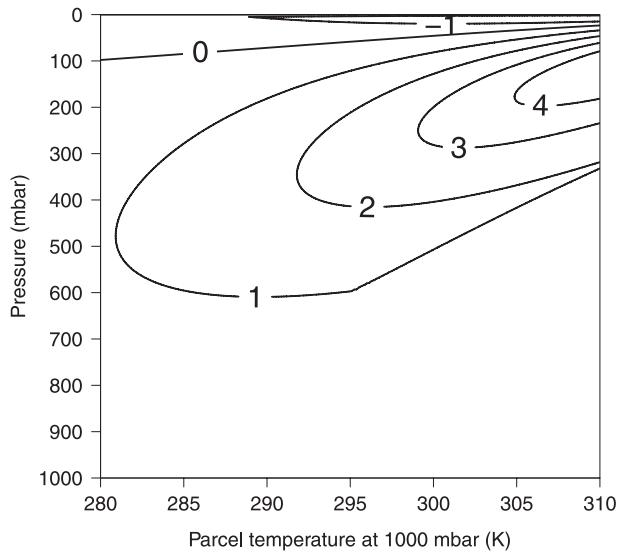
FIG. 9. Contribution from fusion to the temperature of an adiabatic parcel beginning at a surface pressure of 1 bar and a relative humidity of 80%.

FIG. 10. Contribution to CAPE from 1000 to 100 mb for a parcel with an initial relative humidity of 80%.

by as much as 3 K between 300 and 200 mb. However, by the time the parcel has reached 100 mb, its temperature excess over a similar parcel with no fusion is reduced to only 1 K. For a LNB near the cold-point tropopause, where the lapse rate is zero, this corresponds to a difference in LNB of only 100 m.

Although the level of neutral buoyancy is not much affected by fusion, the amount of CAPE is. For the set of initial parcels used to make Fig. 9 (280 to 310 K at 1 bar and 80% relative humidity), Fig. 10 shows the contribution from fusion to CAPE for ascent from 1 bar to 100 mb. The contribution from fusion to CAPE is quite large, ranging from 330 J kg^{-1} at 280 K to around 1400 J kg^{-1} between 306 and 310 K. As we will see, this increase in CAPE from fusion plays an important role in getting clouds to the tropopause.

6. Getting to the tropopause

If even undiluted parcels have a level of neutral buoyancy below the tropopause, how do diluted updrafts manage to get there? One possible answer is that the plumes begin with a higher value of θ_e than the mean θ_e^* at the cloud base. For the diluted plume at the tropopause in the 200-m run, we can diagnose its cloud-base properties using the tracers. Dividing the temperature tracer and the water vapor tracer by the purity, we find that the plume had a temperature of 288.6 K and a water vapor mass fraction of 0.0113 at the cloud base. This corresponds to a θ_e of 328.4 K, exactly equal to the mean value of θ_e^* at the cloud base during the corresponding
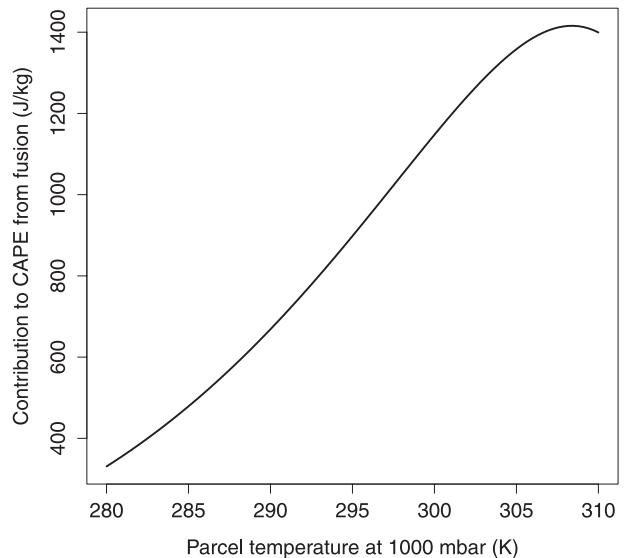
6-h interval. Therefore, an anomalously large θ_e is not the answer.

The only remaining explanation is that the plume got to the tropopause by overshooting its level of neutral buoyancy. Despite the near certainty of this conclusion, it would still be reassuring to demonstrate in a simple model that the plume could have acquired the requisite amount of kinetic energy despite entraining motionless air, losing much of its condensation to fallout, and fighting against drag. Furthermore, we would like to assess whether or not the latent heat of fusion plays an important role, as argued by Zipser (2003) and Fierro et al. (2009). For these purposes, we have constructed a model of an entraining Lagrangian parcel that integrates the prognostic equations for the parcel's volume, mass, water vapor, liquid water, solid water, momentum, and temperature. To mimic observations of supercooled water in deep convective clouds, we have specified that the parcel transition linearly from a warm cloud to a cold cloud between T_{trip} and 240 K. To give behavior halfway between adiabatic and pseudoadiabatic, fallout of precipitation is specified as half the rate of condensation and deposition. The drag force is modeled using the standard definition of the drag coefficient,

$$F_{\text{drag}} \equiv \frac{1}{2} c_d A \rho_e w^2,$$

where ρ_e is the density of the environment; the projected area A is calculated by assuming the parcel is a spherical bubble. The model is specified in more detail in the appendix.
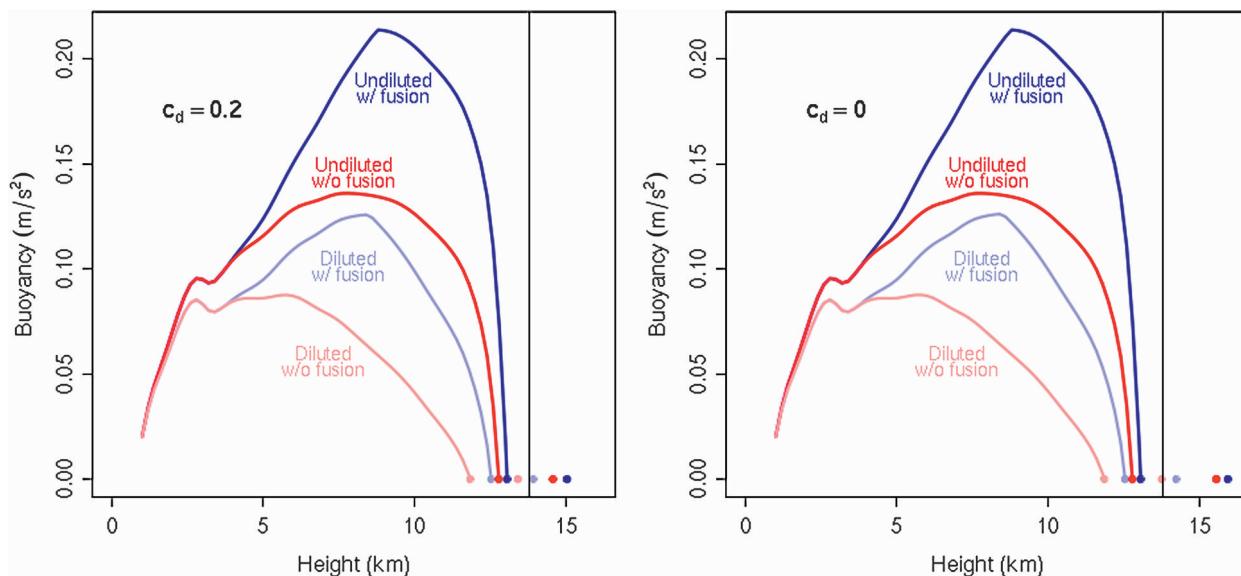
FIG. 11. Buoyancy of parcels in the Lagrangian parcel model using a drag coefficient of (left) 0.2 and (right) 0. The pastel-colored curves (pink and light blue) use an entrainment rate of 5.33×10^{-5} m^{-1}; the primary-colored curves (red and blue) do not entrain at all. The bluish curves (blue and light blue) include an ice phase; the reddish curves (red and pink) do not. The circles at the end of the curves indicate the levels of neutral buoyancy; the other circles indicate the levels to which the parcels overshoot.

We use this model to simulate a parcel traveling through the mean atmospheric profiles of the 200-m simulation. The parcel is initialized using the diagnosed cloud-base properties of the cloudy updraft found at the tropopause. Since this model integrates the momentum equation, we need a cloud-base vertical velocity. Using the tracer that encodes the cloud-base vertical velocity, we are able to diagnose the cloud-base speed as 2.4 m s^{-1}. To initialize the volume, we choose a volume of one cubic kilometer based on the 1-km height of the cloud base. It is also necessary to choose a drag coefficient for the momentum equation. For a spherical bubble with a 1-km diameter and a 10 m s^{-1} speed at 500 mb, the Reynolds number is about 3×10^{8} m^{2} s^{-1}. Empirical studies have found that the minimum drag coefficient for a sphere occurs at the critical Reynolds number for drag crisis (Re $= 1 \sim 5 \times 10^{5}$) at which the drag coefficient drops to about 0.1 (Blevins 1992). At the highest Reynolds number for which drag data are available, Re $= 5 \times 10^{6}$, the drag coefficient is about 0.2. Therefore, we use $c_d = 0.2$.

As in the adiabatic case, four different cases are simulated: with and without an entrainment rate of 5.33×10^{-5} m^{-1} and with and without fusion. The profiles of buoyancy for the four runs are shown in the left panel of Fig. 11. The circles at which the curves terminate denote the levels of neutral buoyancy, all of which are well below the tropopause, confirming the conclusion from the previous section. The circles to the right of the buoyancy curves in Fig. 11 indicate the heights that the

parcels reach by overshooting. Both of the undiluted parcels, with or without fusion, easily surpass the tropopause. The entraining trajectory with fusion just barely reaches the tropopause, just as in the cloud-resolving simulation. On the other hand, the entraining trajectory without fusion falls short. This supports the claim, made by Zipser (2003) and Fierro et al. (2009), that fusion plays a critical role in getting diluted plumes to the tropopause.

To test the robustness of this result to changes in parcel size and drag coefficient, we have repeated the calculations using $c_d = 0$, which will allow parcels to convert more of their CAPE to kinetic energy. The right panel of Fig. 11 shows the four buoyancy profiles when $c_d = 0$. Of course, the buoyancy profiles are the same between the two panels of Fig. 11 because the change in drag alters momentum, not thermodynamics. On the other hand, the velocity profiles, displayed side by side in Fig. 12, are quite different for $c_d = 0.2$ and $c_d = 0$. Note that the entraining parcel without fusion still fails to reach the tropopause even in the unphysical scenario of zero drag. In this simple model, the limit of $c_d \to 0$ is the same as the limit of $V \to \infty$, where V is the volume of the parcel. Therefore, there is no drag coefficient or initial volume that would allow the entraining parcel to reach the tropopause.

Finally, we test the sensitivity of the results to the fraction of condensates allowed to fall out of the parcel. We contemplate two extremes: in one case, all condensates are retained, and, in the other, condensates are removed immediately upon formation. Using a drag
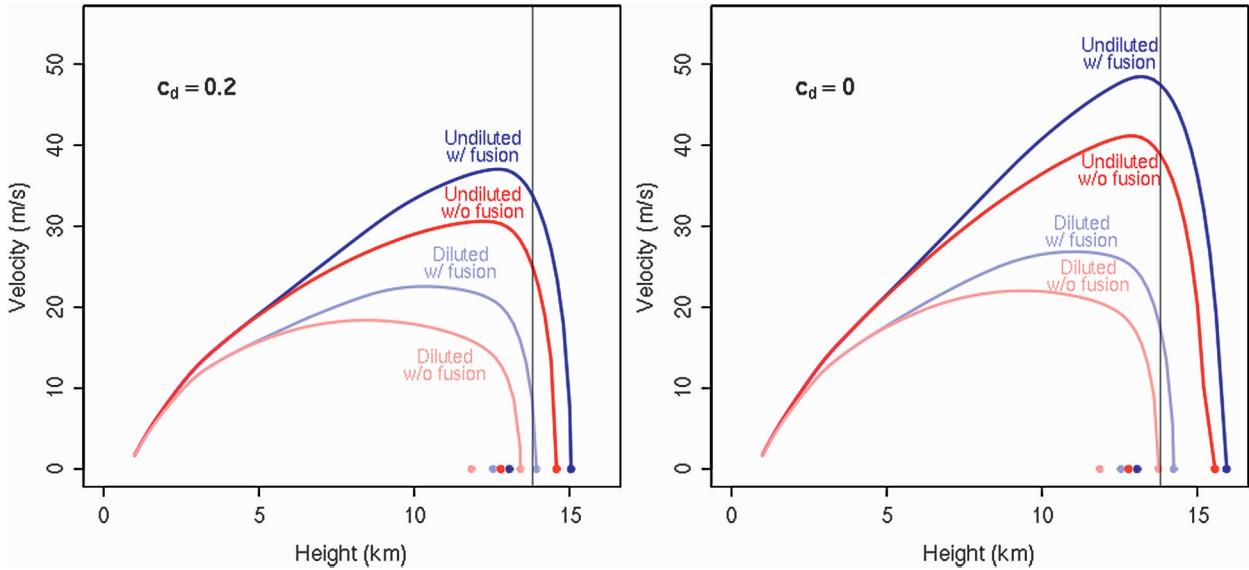
FIG. 12. As in Fig. 11 but for vertical velocity instead of buoyancy.

coefficient of $c_d = 0.2$ and an initial volume of a cubic kilometer, Fig. 13 shows the overshooting heights for the "no fallout" case on the left and the "total fallout" case on the right. Since the parcels without fusion (reddish points) do not gain any buoyancy from the freezing of

their liquid condensates, those condensates serve mainly to weigh the parcel down. When the condensates are allowed to fall out, the overshooting height increases by about one kilometer. Note, though, that the diluted parcel without fusion still misses the tropopause even in
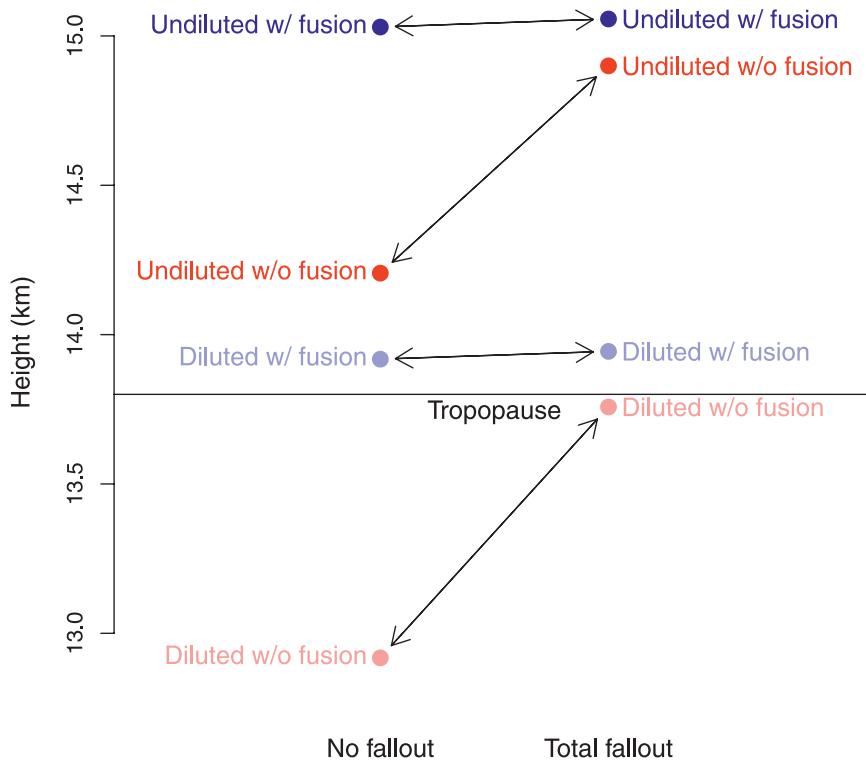

FIG. 13. The overshooting height of parcels with $c_d = 0.2$: (left) heights with no fallout of condensates; (right) heights with immediate fallout of all condensates.

the case of total fallout. On the other hand, the parcels with fusion (bluish points) do just as well with and without the retention of their condensates. This is due to a rough cancellation between the weight of the condensates and the buoyancy source produced by the freezing of the condensates (Williams and Renno 1993). Therefore, the retention of condensates is neither a help nor a hindrance to these overshooting parcels with fusion.

7. Conclusions

The simulations presented here suggest that, in radiative–convective equilibrium, the flux of undiluted plumes above 4–5 km is negligible. It worth noting that this result was obtained for a very generous definition of "undiluted" whereby any parcel with a purity above 80% qualified; as the purity threshold is increased, the flux of undiluted parcels becomes even more negligible. Although these simulations were performed at a resolution likely greater than that needed to resolve the inertial subrange, there was no discernible trend in the undiluted flux over a range of horizontal resolutions from 3.2 km to 100 m. This suggests that the absence of deep undiluted parcels can be extrapolated to a higher resolution and, therefore, to the real tropical atmosphere.

The distribution of undiluted flux with height takes a particularly simple form that lends itself to easy implementation in a convective parameterization. The undiluted cloud flux decays with height exponentially with a decay coefficient equal to about 1.85 ± 0.25 km^{-1} for the 80% threshold. Although there is some variability of the decay coefficient within this range among the simulations, there is no systematic trend with increasing resolution. This suggests that a decay parameter in this range might be appropriate for parameterizations.

Despite the absence of undiluted plumes in the upper troposphere in the cloud-resolving simulations, convection does reach to the tropopause. Using an ensemble of tracers, it is possible to show that plumes can reach the tropopause without the benefit of an anomalously large initial θ_e. Instead, as originally argued by Zipser (2003), fusion appears to be the key. Although fusion provides very little of any boost in the final level of neutral buoyancy, it supplies a great deal of CAPE, which enables diluted parcels to overshoot to the tropopause.

APPENDIX

The Lagrangian Parcel Model

To specify the Lagrangian parcel model, let us define V, ρ, q_v, q_l, q_s, and w as the parcel's volume, density, water mass fractions (vapor, liquid, and solid), and vertical velocity. We also define E^{tot} as the specific total energy of the parcel,

$$E^{tot} = c_{vm}(T - T_{trip}) + q_v E_{0v} - q_s E_{0s} + \frac{1}{2}w^2 + gz,$$

comprising its internal energy, kinetic energy, and gravitational potential energy. Here c_{vm} is the specific heat capacity at constant volume for the moist parcel,

$$c_{vm} = (1 - q_v - q_l - q_s)c_{va} + q_v c_{vv} + q_l c_{vl} + q_s c_{vs}.$$

The governing equations for the parcel's volume, total mass, vapor mass, liquid mass, solid mass, momentum, and total energy are

$$d_t V = V\psi + \frac{V\epsilon}{\rho_e} - \frac{V\delta}{\rho};$$

$$d_t(V\rho) = -Vf_l - Vf_s + V\epsilon - V\delta;$$

$$d_t(V\rho q_v) = Ve + V\epsilon q_{ve} - V\delta q_v;$$

$$d_t(V\rho q_l) = -Ve + Vm - V\delta q_l - Vf_l;$$

$$d_t(V\rho q_s) = -Vm - V\delta q_s - Vf_s;$$

$$d_t(V\rho w) = -V\rho g - V\partial_z p - V\delta w - V(f_l + f_s)w$$
$$- \frac{1}{2}d_t(V\rho_e w) - \frac{1}{4}V\left(\frac{9\pi}{2V}\right)^{1/3}c_d\rho_e w^2;$$

$$d_t(V\rho E^{tot}) = V\epsilon E_e^{tot} - V\delta E^{tot} - Vw\partial_z p - Vp\psi$$
$$- Vf_l E_l^{tot} - Vf_s E_s^{tot} - \frac{1}{2}w d_t(V\rho_e w)$$
$$- \frac{1}{4}V\left(\frac{9\pi}{2V}\right)^{1/3}c_d\rho_e w^3.$$

On the right-hand sides of these equations are ϵ (the mass entrainment rate), δ (the mass detrainment rate), f_l (the liquid-mass fallout rate), f_s (the solid-mass fallout rate), e (the microphysical vapor mass source—i.e., evaporation), and m (the microphysical solid mass sink—i.e., melting), which all have dimensions of mass per time per parcel volume. On the right-hand side of the volume equation, ψ is the parcel's fractional expansion rate and the mass rates of entrainment and detrainment have been converted to volume rates by dividing by ρ_e (the density of environmental air) and ρ, respectively. The total energies with subscripts l, s, and e are the total specific energies of liquid water, solid water, and environmental air,

$$E_l^{\text{tot}} = c_{vl}(T - T_{\text{trip}}) + \frac{1}{2}w^2 + gz;$$

$$E_s^{\text{tot}} = c_{vs}(T - T_{\text{trip}}) + \frac{1}{2}w^2 + gz - E_{0s};$$

$$E_e^{\text{tot}} = c_{vme}(T_e - T_{\text{trip}}) + gz + q_{ve}E_{0v},$$

where the subscript e denotes properties of the environmental air. The second-to-last term in the momentum equation is the force felt by the parcel as it accelerates the environmental air around it, which, for a sphere, is equivalent to accelerating one half of the displaced mass (see, e.g., Batchelor 2005). The last term of the momentum equation is the drag force expressed using the standard definition of the drag coefficient,

$$F_{\text{drag}} \equiv \frac{1}{2}c_d(\text{projected area})\rho_e w^2,$$

and assuming that the parcel is a spherical bubble. The work performed by the parcel accelerating environmental air or fighting drag is energy transferred to the environment, as reflected by the last two terms in the energy equation.

Since we are interested in a parcel that only detrains at its level of neutral buoyancy, we set $\delta = 0$. The governing equations may then be manipulated algebraically to yield

$$d_t V = V\psi + \frac{V\epsilon}{\rho_e};$$

$$d_t\rho = -f_l - f_s + \epsilon\left(1 - \frac{\rho}{\rho_e}\right) - \rho\psi;$$

$$\rho d_t q_v = e + (f_l + f_s)q_v + \epsilon(q_{ve} - q_v);$$

$$\rho d_t q_l = -e + m - f_l + (f_l + f_s)q_l - \epsilon q_l;$$

$$\rho d_t q_s = -m - f_s + (f_l + f_s)q_s - \epsilon q_s;$$

$$\left(\rho + \frac{1}{2}\rho_e\right)d_t w = -\rho g - \partial_z p - \frac{3}{2}\epsilon w - \frac{1}{2}\rho_e w\psi$$
$$- \frac{1}{2}w^2\partial_z\rho_e - \frac{1}{4}\left(\frac{9\pi}{2V}\right)^{1/3}c_d\rho_e w^2;$$

$$\rho c_{pm}d_t T = d_t p - L_e e - L_m m + \epsilon c_{pme}(T_e - T)$$
$$+ \frac{1}{2}\epsilon w^2;$$

$$p\psi = -\frac{c_{vm}}{c_{pm}}d_t p + R_v T e - \epsilon R_{me}(T_e - T)$$
$$+ \frac{R_m}{c_{pm}}\left[-L_e e - L_m m\right.$$
$$+ \epsilon c_{pme}(T_e - T) + \frac{1}{2}w^2\right].$$

Given a specification for ϵ; supplying microphysical equations for $e, m, f_l,$ and f_s; and using the facts that $p = p_e$ and $d_t z = w$, we have a closed set of equations with which to integrate the trajectory of an entraining parcel.

To specify e and m, we must define the saturation vapor pressure and the apportionment of condensates into liquid and solid. Since condensates are not observed to freeze entirely until about 240 K, we define

$$q_v^* = (1 - \xi(T))q_v^{*,l} + \xi(T)q_v^{*,s};$$
$$q_l = (1 - \xi(T))(q_l + q_s);$$
$$q_s = \xi(T)(q_l + q_s),$$

with

$$\xi = \begin{cases} 1, & T \le 240 \\ \dfrac{T_{\text{trip}} - T}{T_{\text{trip}} - 240}, & 240 < T < T_{\text{trip}} \\ 0, & T \ge T_{\text{trip}}. \end{cases}$$

Furthermore, we assume that condensates fall out at a rate proportional to the rate of condensation and deposition:

$$f_l = \gamma\max(0, -e)\frac{q_l}{q_l + q_s};$$
$$f_s = \gamma\max(0, -e)\frac{q_s}{q_l + q_s}.$$

In all the integrations performed here, we have used $\gamma = 0.5$, which is halfway between adiabatic and pseudoadiabatic.

REFERENCES

Batchelor, G. K., 2005: *An Introduction to Fluid Dynamics*. Cambridge University Press, 615 pp.

Blevins, R. D., 1992: *Applied Fluid Dynamics Handbook*. Krieger, 558 pp.

Bretherton, C. S., and P. K. Smolarkiewicz, 1989: Gravity waves, compensating subsidence, and detrainment around cumulus clouds. *J. Atmos. Sci.,* **46,** 740–759.

Bryan, G. H., J. C. Wyngaard, and J. M. Fritsch, 2003: Resolution requirements for the simulation of deep moist convection. *Mon. Wea. Rev.,* **131,** 2394–2416.

Clough, S., M. Shephard, E. Mlawer, J. Delamere, M. Iacono, K. Cady-Pereira, S. Boukabara, and P. Brown, 2005: Atmospheric radiative transfer modeling: A summary of the AER codes. *J. Quant. Spectrosc. Radiat. Transfer,* **91,** 233–244.

Cohen, C., 2000: A quantitative investigation of entrainment and detrainment in numerically simulated cumulonimbus clouds. *J. Atmos. Sci.,* **57,** 1657–1674.

Emanuel, K. A., 1994: *Atmospheric Convection*. Oxford University Press, 580 pp.

——, and M. Živković-Rothman, 1999: Development and evaluation of a convection scheme for use in climate models. *J. Atmos. Sci.,* **56,** 1766–1782.

Fierro, A. O., J. M. Simpson, M. A. Lemone, J. M. Straka, and B. F. Smull, 2009: On how hot towers fuel the Hadley cell: An observational and modeling study of line-organized convection in the equatorial trough from TOGA COARE. *J. Atmos. Sci.,* **66,** 2730–2746.

Hauf, T., and H. Höller, 1987: Entropy and potential temperature. *J. Atmos. Sci.,* **44,** 2887–2901.

Heymsfield, A., P. Johnson, and J. Dye, 1978: Observations of moist adiabatic ascent in northeast Colorado cumulus congestus clouds. *J. Atmos. Sci.,* **35,** 1689–1703.

Iacono, M., J. Delamere, E. Mlawer, M. Shephard, S. Clough, and W. Collins, 2008: Radiative forcing by long-lived greenhouse gases: Calculations with the AER radiative transfer models. *J. Geophys. Res.,* **113,** D13103, doi:10.1029/2008JD009944.

Jensen, J., P. Austin, M. Baker, and A. Blyth, 1985: Turbulent mixing, spectral evolution, and dynamics in a warm cumulus cloud. *J. Atmos. Sci.,* **42,** 173–192.

Kain, J., and J. Fritsch, 1990: A one-dimensional entraining/detraining plume model and its application in convective parameterization. *J. Atmos. Sci.,* **47,** 2784–2802.

Klemp, J. B., W. C. Skamarock, and J. Dudhia, 2007: Conservative split-explicit time integration methods for the compressible nonhydrostatic equations. *Mon. Wea. Rev.,* **135,** 2897–2913.

Kley, D., P. Crutzen, H. Smit, H. Vömel, S. Oltmans, H. Grassl, and V. Ramanathan, 1996: Observations of near-zero ozone concentrations over the convective Pacific: Effects on air chemistry. *Science,* **274,** 230–233.

Krueger, S., Q. Fu, K. Liou, and H. Chin, 1995: Improvements of an ice-phase microphysics parameterization for use in numerical simulations of tropical convection. *J. Appl. Meteor.,* **34,** 281–287.

Kuang, Z., and C. Bretherton, 2006: A mass-flux scheme view of a high-resolution simulation of a transition from shallow to deep cumulus convection. *J. Atmos. Sci.,* **63,** 1895–1909.

LeMone, M., and E. Zipser, 1980: Cumulonimbus vertical velocity events in GATE. Part I: Diameter, intensity, and mass flux. *J. Atmos. Sci.,* **37,** 2444–2457.

Lin, Y., R. Farley, and H. Orville, 1983: Bulk parameterization of the snow field in a cloud model. *J. Climate Appl. Meteor.,* **22,** 1065–1092.

Lord, S., H. Willoughby, and J. Piotrowicz, 1984: Role of a parameterized ice-phase microphysics in an axisymmetric, nonhydrostatic tropical cyclone model. *J. Atmos. Sci.,* **41,** 2836–2848.

MacPherson, J., and G. Isaac, 1977: Turbulent characteristics of some Canadian cumulus clouds. *J. Appl. Meteor.,* **16,** 81–90.

Paluch, I., 1979: The entrainment mechanism in Colorado cumuli. *J. Atmos. Sci.,* **36,** 2467–2478.

Raymond, D., and A. Blyth, 1986: A stochastic mixing model for nonprecipitating cumulus clouds. *J. Atmos. Sci.,* **43,** 2708–2718.

Riehl, H., and J. Malkus, 1958: On the heat balance in the equatorial trough zone. *Geophysica,* **6,** 503–538.

Romps, D. M., 2008: The dry-entropy budget of a moist atmosphere. *J. Atmos. Sci.,* **65,** 3779–3799.

Siebesma, A., and J. Cuijpers, 1995: Evaluation of parametric assumptions for shallow cumulus convection. *J. Atmos. Sci.,* **52,** 650–666.

——, and A. Holtslag, 1996: Model impacts of entrainment and detrainment rates in shallow cumulus convection. *J. Atmos. Sci.,* **53,** 2354–2364.

Wang, C., and R. Prinn, 2000: On the roles of deep convective clouds in tropospheric chemistry. *J. Geophys. Res.,* **105** (D17), 22 269–22 297.

Williams, E., and N. Renno, 1993: An analysis of the conditional instability of the tropical atmosphere. *Mon. Wea. Rev.,* **121,** 21–36.

Xu, K., and K. Emanuel, 1989: Is the tropical atmosphere conditionally unstable? *Mon. Wea. Rev.,* **117,** 1471–1479.

Yasunaga, K., H. Kida, T. Satomura, and N. Nishi, 2004: A numerical study on the detrainment of tracers by cumulus convection in TOGA COARE. *J. Meteor. Soc. Japan,* **82,** 861–878.

Zipser, E. J., 2003: Some views on hot towers after 50 years of tropical field programs and two years of TRMM data. *Cloud Systems, Hurricanes, and the Tropical Rainfall Measuring Mission (TRMM): A Tribute to Dr. Joanne Simpson, Meteor. Monogr.,* No. 51, Amer. Meteor. Soc., 50–59.